

Superiorized polyenergetic reconstruction algorithm for reduction of metal artifacts in CT images

T. Humphries¹ and A. Gibali²

Abstract—Artifacts caused by metal objects such as dental fillings, hip implants, and coronary stents are a significant source of error in many CT scans. These artifacts are caused by numerous factors, including beam hardening, noise, photon starvation, partial volume and exponential edge gradient effects, and scatter. We propose an iterative algorithm for CT image reconstruction which reduces these artifacts. The algorithm does so by (1) accurately modeling polyenergetic X-ray data, (2) statistically weighting the X-ray data to reduce the effect of noisy measurements, and (3) incorporating total variation (TV) as a secondary objective. The recently proposed superiorization methodology provides a solid mathematical foundation for our approach. Our numerical experiments indicate that all three of these features of the algorithm play an important role in reducing metal artifacts.

I. INTRODUCTION

Metal artifacts are caused by numerous factors, including beam hardening, noise, photon starvation, partial volume and exponential edge gradient effects (EEGE), and scatter [1]. Typical artifacts include dark streaking between regions containing metal, as well as thin, alternating dark and light streaks emanating from the metal regions. The former are caused primarily by beam hardening and photon starvation, while the latter are due mainly to noise and EEGE.

Fig. 1 illustrates these different artifacts in a numerical phantom experiment. The upper right image was reconstructed from noiseless, monoenergetic data using the simultaneous algebraic reconstruction technique (SART). We see that even in this ideal case there are streaking artifacts around the metal objects caused by geometric inconsistency between the data and the forward model used by SART. There are also some dark shadows around the metal objects, although these artifacts are diminished by further iterations of the algorithm. The bottom left image shows that when the X-ray data are polyenergetic, there are severe streaking artifacts between high-attenuation materials (bone and metal) due to beam hardening. The addition of noise to the data (bottom right image) produces even more severe streaking, which makes it impossible to see the central features of the object.

To address these different sources of error, we propose an iterative algorithm for CT image reconstruction which reduces metal artifacts. The algorithm does so by (1) accurately modeling polyenergetic X-ray data, (2) statistically weighting the X-ray data to reduce the effect of noisy measurements, and (3) incorporating total variation (TV) as a secondary objective. Our numerical experiments indicate that all three

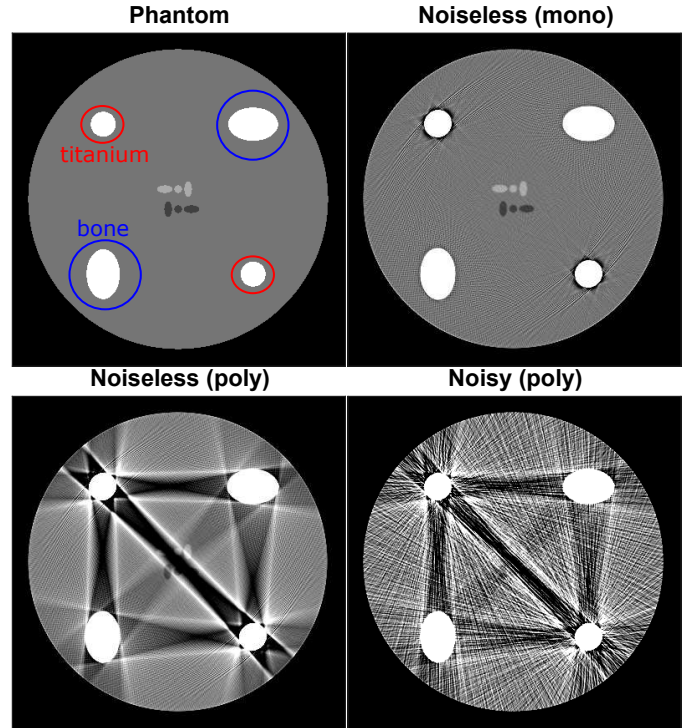


Fig. 1. Images of phantom containing metal objects, reconstructed using 32 iterations of SART with 12 subsets. Top left: True phantom at reference energy of 70 keV. Top right: Image reconstructed from noiseless monoenergetic data. Bottom left: Image reconstructed from noiseless polyenergetic data that has been soft tissue corrected. Bottom right: Image reconstructed from noisy polyenergetic soft tissue corrected data. All images are displayed on greyscale window $[0.18, 0.23] \text{ cm}^{-1}$ to show low-contrast features.

of these features of the algorithm play an important role in reducing metal artifacts. The recently proposed superiorization methodology [2] provides a solid mathematical foundation for our approach.

II. METHODOLOGY

A. Mathematical model

We let $\mu(\mathbf{y}, E)$ represent the distribution of attenuation as a function of position \mathbf{y} and energy, E . A polyenergetic X-ray measurement along the line j is modeled as:

$$\hat{I}_j = \int S(E) \exp\left(-\int_j \mu(\mathbf{y}, E) d\mathbf{y}\right) dE, \quad (1)$$

where $S(E)$ is the spectrum of the beam as a function of energy. For monoenergetic data, we have $S(E) = I_0\delta(E-E_0)$ for some energy E_0 and total intensity I_0 , and (1) can be

¹ School of STEM, University of Washington Bothell, Bothell, WA, USA

² Department of Mathematics, ORT Braude College, Karmiel, Israel

linearized as

$$-\ln\left(\widehat{I}_j/I_0\right) = \int_j \mu(\mathbf{y}, E_0) d\mathbf{y} \quad (2)$$

To reconstruct μ iteratively, we discretize it as an $n \times n$ pixel image. Assuming we collect a total of J measurements, and letting $K = n^2$, Eq. (2) can be represented as

$$\mathbf{b} = A\mathbf{x}, \quad (3)$$

where $\mathbf{x} \in \mathbb{R}^K$ represents the image of μ , $\mathbf{b} \in \mathbb{R}^J$ is the log-transformed projection data, and $A \in \mathbb{R}^{J \times K}$ is the system matrix.

Iterative methods such as the simultaneous algebraic reconstruction technique (SART) can be applied to solve (3). In the polyenergetic case, SART can be applied to log-transformed data in the same way, but the inconsistency of (1) with the linear model produces beam hardening artifacts. Soft tissue correction may be applied in this case, but this is only effective in reducing cupping artifacts.

Noise is modeled by drawing each polyenergetic measurement I_j from a Poisson distribution with mean equal to \widehat{I}_j . The signal-to-noise ratio (SNR) of measurement I_j decreases with \widehat{I}_j , i.e. if the beam experiences more attenuation along the line j . Photon starvation arises when \widehat{I}_j is so small that I_j may be zero. This corresponds to ‘‘infinite’’ attenuation along the line j , which cannot be modeled in Eq. (3). In our experiments we set $I_j = 1$ in such cases, i.e., a single photon count. This avoids the issue of singularity, but the altered data do not accurately reflect the object attenuation along that line.

B. Numerical methods

BI-SART: We first introduce a block-iterative variant of SART, denoted BI-SART, as the basic algorithm. Following [3], we define the following two diagonal matrices D and M :

$$D \in \mathbb{R}^{K \times K}, \quad D_{kk} = \frac{1}{\zeta_k}, \quad \zeta_k = \sum_{i=1}^m |a_{ik}|, \quad k = 1 \dots K$$

$$M \in \mathbb{R}^{J \times J}, \quad M_{jj} = \frac{1}{\eta_j}, \quad \eta_j = \sum_{i=1}^n |a_{ji}|, \quad j = 1 \dots J$$

That is, the entries of D are formed by reciprocals of the column sums of A , while the entries of M are formed by row sums. We also partition the measurements corresponding to each angular view into N_w subsets, indexed by w . This block-iterative approach (also known as ordered subsets) accelerates the convergence of the algorithm. We then define BI-SART as

$$\mathbf{x}^{(i+1)} = \mathbf{Q}\mathbf{B}_{N_w} \dots \mathbf{B}_2\mathbf{B}_1(\mathbf{x}^{(i)}), \text{ where} \quad (4)$$

$$\mathbf{B}_w(\mathbf{x}) = \mathbf{x} - D_w(A_w)^T M_w [A_w \mathbf{x} - \mathbf{b}_w], \quad (5)$$

and $(\mathbf{Q}\mathbf{x})_k = \max\{0, x_j\}, \quad k \in [1, K]$.

The subscript w indicates that only rows of A and \mathbf{b} corresponding to the measurements in w are used, including when forming the matrices D_w and M_w . The operator \mathbf{Q} ensures non-negativity of the entries of \mathbf{x} . We now consider three potential enhancements to this basic algorithm.

1) *Polyenergetic forward model:* A polyenergetic forward projection is achieved using linear interpolation between tabulated attenuation curves for known basis materials such as soft tissue, bone, and metal [4]. This algorithm, which we denote as BI-pSART, has the same form as BI-SART (4), but with

$$\mathbf{B}_w(\mathbf{x}) = \mathbf{x} - D_w(A_w)^T M_w [\mathcal{P}_w(\mathbf{x}) - \mathbf{b}_w], \text{ where} \quad (6)$$

$$[\mathcal{P}(\mathbf{x})]_j = -\ln \left[\sum_{h=1}^{N_h} S_h \exp(-a_j \mu(\mathbf{x}, E_h)) \right] / \sum_{h=1}^{N_h} S_h, \text{ and} \quad (7)$$

$$\mu(x_k, E) = \frac{[\mu_{m+1}(E_0) - x_k]\mu_m(E) + [x_k - \mu_m(E_0)]\mu_{m+1}(E)}{\mu_{m+1}(E_0) - \mu_m(E_0)}. \quad (8)$$

Here S_h represents a discretization of the beam spectrum $S(E)$ into N_h energy levels, and a_j is the j th row of A . The vector \mathbf{x} now represents the attenuation map at the reference energy E_0 , while $\mu_m(E)$ and $\mu_{m+1}(E)$ are the tabulated linear attenuation coefficient (LAC) functions of the two basis materials whose LACs at E_0 bracket the value of x_k . Thus if x_k has a value between the LAC of soft tissue and bone at E_0 , then the energy-dependent LAC of pixel k is determined by linear interpolation according to (8). BI-pSART is a nonlinear fixed-point iteration whose convergence properties have been studied in [5].

2) *Weighted least squares:* As noise is a significant contributor to metal artifacts, we employ a weighted least squares (WLS) technique [6] to more strongly weight measurements with higher SNR. We define a $J \times J$ diagonal weighting matrix by $\{W^{\frac{1}{2}}\}_{jj} = \sqrt{I_j}$. We then replace (5) with

$$\mathbf{B}_w(\mathbf{x}) = \mathbf{x} - D'_w(A_w)^T M_w \left[W^{\frac{1}{2}} (A_w(\mathbf{x}) - \mathbf{b}_w) \right], \quad (9)$$

$$\text{where } D'_{jj} = \frac{1}{\zeta'_j}, \quad \zeta'_j = \sum_{i=1}^m \left| (W^{\frac{1}{2}} A)_{ik} \right|, \quad j = 1 \dots J$$

This equates to applying BI-SART to the system $W^{\frac{1}{2}} A \mathbf{x} = W^{\frac{1}{2}} \mathbf{b}$. It is not necessary to modify the matrix M in (9), as multiplying A by $W^{\frac{1}{2}}$ has the effect of multiplying M by $W^{-\frac{1}{2}}$, the effect of which is then cancelled by multiplication with $(W^{\frac{1}{2}} A)^T$.

3) *TV-superiorization:* Superiorization [2] is an optimization heuristic in which an iterative algorithm is *superiorized* by perturbing the solution within each iteration, in order to improve it with respect to some objective function, $\phi(\mathbf{x})$. In this instance, we superiorize BI-SART by replacing (4) with

$$\mathbf{x}^{(i+1)} = \mathbf{Q}\mathbf{B}_{N_w} \dots \mathbf{B}_2\mathbf{B}_1(\mathbf{x}^{(i)} + \beta_i \mathbf{v}_i). \quad (10)$$

The step sizes, β_i , are required to be a summable sequence (e.g. $\beta_i = \gamma^i, 0 \ll \gamma < 1$), and the \mathbf{v}_i are chosen to be non-ascending directions of the secondary objective, e.g. $-\nabla \phi(\mathbf{x}_i)$. The principle of superiorization is that if the basic algorithm is *perturbation resilient*, then the superiorized algorithm will eventually find a solution that is as satisfactory as that found by the basic algorithm with respect to solving the inverse problem. Due to the perturbations introduced at each iteration, it is also expected that this solution will be superior with respect to the secondary objective.

In this work we choose this objective to be the total variation (TV) of the image:

$$\phi_{TV}(\mathbf{x}) = \sum_{m,n} \sqrt{(x_{m+1,n} - x_{m,n})^2 + (x_{m,n+1} - x_{m,n})^2 + \epsilon^2},$$

where $x_{m,n}$ denotes the pixel in the m th row and n th column of the image \mathbf{x} , and ϵ is a small parameter introduced to avoid singularity of $\nabla\phi_{TV}$. The negative gradient is used as the direction \mathbf{v}_i at each iteration. TV-superiorized pSART was previously investigated in [7] for sparse-view and limited-angle CT; it has previously been used for metal artifact reduction or in conjunction with a WLS approach.

III. NUMERICAL EXPERIMENTS

A. Simple phantom

We first present the results of a numerical phantom experiment using a 400×400 pixel phantom (pixel size .75 mm). The phantom consists of a large disc modeling soft tissue, two oblong discs modeling bone, and two small circular discs modeling titanium, as well as several low contrast features in the centre of the object. Noisy polyenergetic parallel beam data (720 views over 180°) were generated analytically using a simulated 130 kVp spectrum, at several different initial beam intensities $I_0 = \int S(E) dE$. The spectrum and attenuation coefficients, as well as the system matrices used for iterative reconstruction, were generated from the Michigan Image Reconstruction Toolbox [8].

Taking BI-SART as the base algorithm, any of the three features described previously (WLS, polyenergetic modeling, and TV-superiorization) can be included or omitted, giving eight possible reconstruction approaches. In Fig. 2 we use the prefix p to denote polyenergetic modeling, W to denote WLS, and the suffix -TV to denote TV superiorization. Data for the images reconstructed without polyenergetic modeling were soft tissue corrected to reduce beam hardening artifacts. The unsuperiorized algorithms were run for 32 iterations with 12 subsets of projection data; the corresponding superiorized algorithms were run until an equally constraints-compatible solution was found (in the sense of minimizing the least-squares error between the measurements and forward projection of the image).

From Fig. 2 it is apparent that all of the images reconstructed without polyenergetic modeling (top row and third row) suffer from severe dark streaking artifacts between bone and metal objects. Noise is also an issue in all of these images, even when TV minimization is included. Only the pSART-TV and WpSART-TV algorithms (second row and fourth row, second and fourth columns) are effective in reducing both beam hardening artifacts and image noise. We observe, however, that the WpSART-TV algorithm is more effective in preserving the resolution of the low-contrast features in the centre of the image. The difference in quality is more apparent at the higher noise level ($I_0 = 2 \times 10^5$, second row) than at the lower noise level (fourth row). This is intuitively sensible as the data along lines passing through both metal objects become extremely noisy as the initial beam intensity diminishes, so the weighting is effective in reducing the effect

of those measurements. Reducing the initial beam intensity beyond $I_0 = 2 \times 10^5$ produced images with significant artifacts for all the reconstruction techniques.

We note that the inclusion of weighting also introduces a dark streak between the metal objects even when using polyenergetic modeling (second and bottom row, third column), which is not present when the weighting is excluded (second and bottom row, first column). This dark streak is not due to beam hardening, but rather occurs as an artifact of the low weight assigned to the measurements passing through both metal objects (in essence, we are missing data along those lines). This artifact is effectively removed by the TV superiorization (bottom row, fourth column), which penalizes the false edges introduced by this streak while having minimal effect on the data consistency.

B. XCAT phantom

To test the approach on a more anatomically realistic phantom, we ran a series of simulations on the XCAT phantom [9]. A 512×512 pixel slice of the phantom (pixel size 0.75mm) was used, with two large titanium objects inserted to simulate a bilateral hip implant. Polyenergetic fan beam data were generated using the analytic XCAT CT projection tool [10] with 1800 views acquired over 360° , and a 140 kVp spectrum. As before, data were generated at several initial count levels. The unsuperiorized algorithms were run for 8 iterations with 60 subsets of projection data; the corresponding superiorized algorithms were run until an equally constraints-compatible solution was found.

The results of this experiment, as shown in Fig. 3, are largely consistent with the simple phantom experiment. The algorithm incorporating all three enhancements (polyenergetic forward projection, weighted least squares, and TV superiorization) is most effective in reducing the artifacts caused by metal. The dark streak between the two metal objects was challenging to remove in this experiment; this was only possible at a high initial intensity of $I_0 = 1 \times 10^7$. The large size of the metal implants caused significant photon starvation at lower beam intensities.

IV. CONCLUSIONS

In this work we present an iterative algorithm for CT reconstruction which aims to reduce artifacts caused by metal objects. Our approach incorporates polyenergetic forward projection, statistical weighting of the X-ray data, and superiorization of the basic algorithm with respect to TV. Numerical phantom experiments indicate that all three of these features play a role in reducing both high and low-frequency streak artifacts caused by metal objects. Further validation of the method will require comparing it to existing techniques for metal artifact reduction, as well as investigating its robustness under additional sources of error such as spectrum mismatch.

REFERENCES

- [1] B De Man, J Nuyts, P Dupont, G Marchal, and P Suetens. Metal streak artifacts in x-ray computed tomography: a simulation study. *IEEE Transactions on Nuclear Science*, 46(3):691–696, 1999.

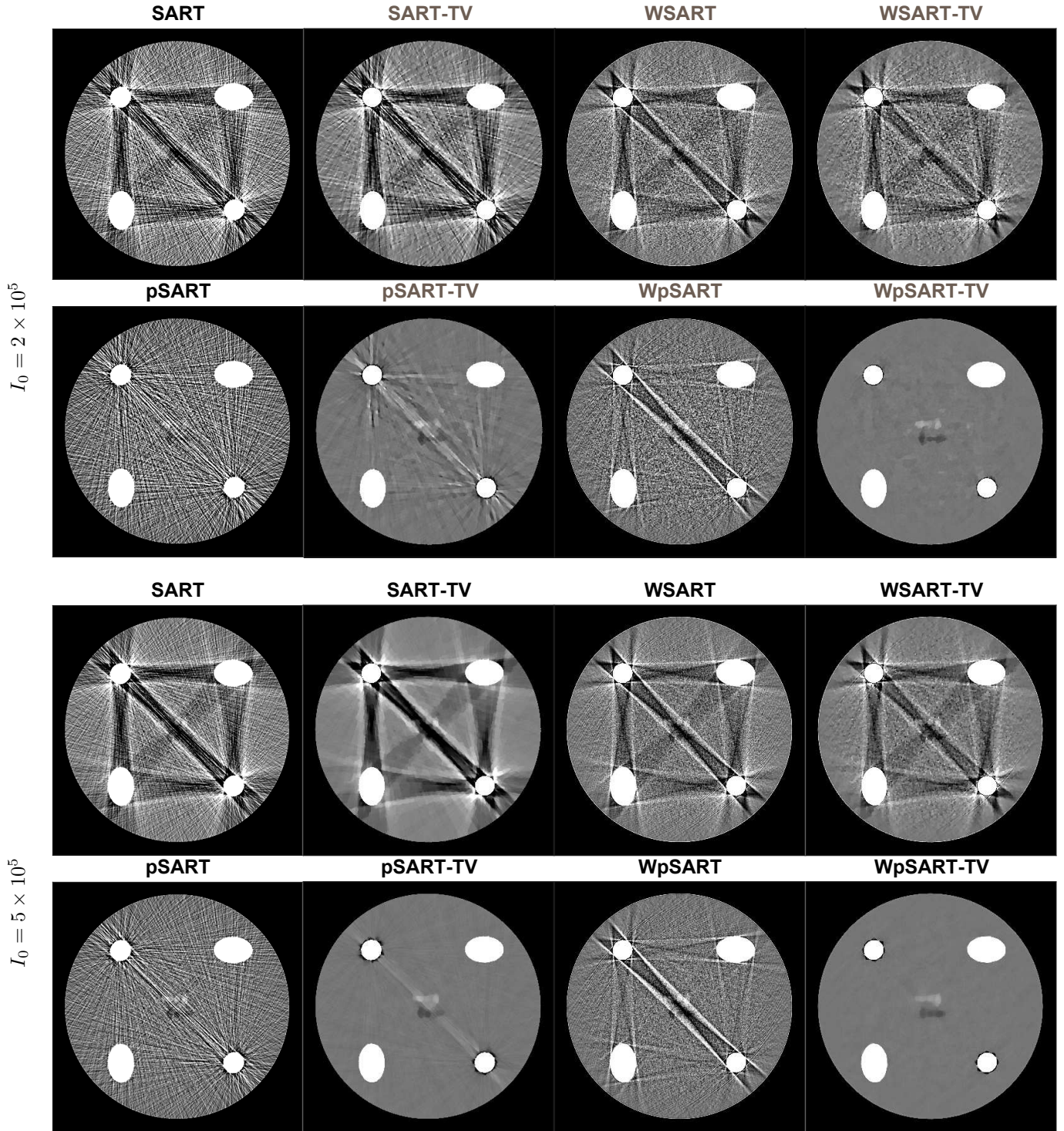


Fig. 2. Images reconstructed of simple phantom at two different noise levels. All figures shown on a greyscale window of $[0.18, 0.23] \text{ cm}^{-1}$ at a reference energy of 70 keV.

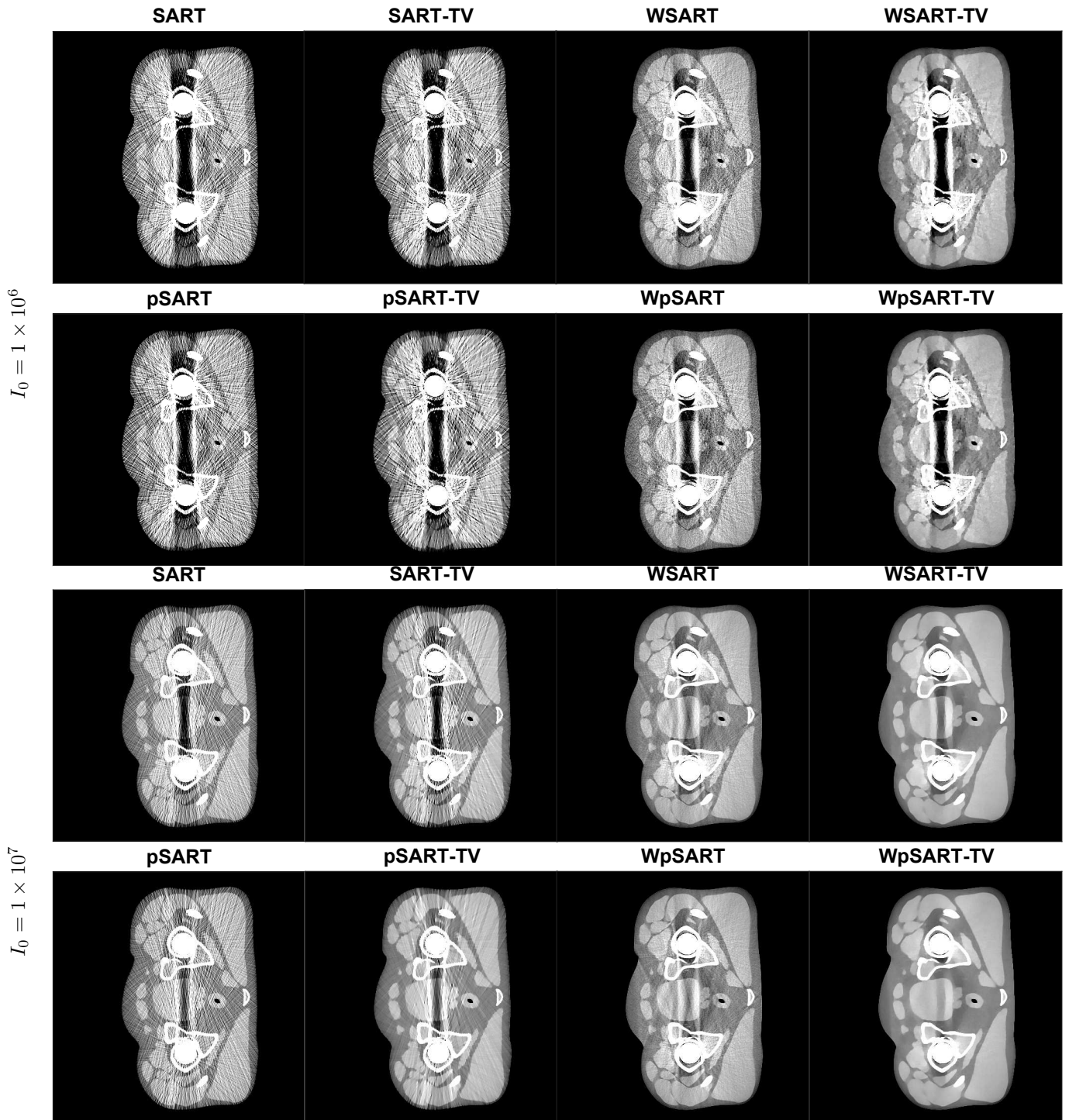


Fig. 3. Images reconstructed of XCAT phantom at two different noise levels. All figures shown on a greyscale window of $[0.1, 0.2] \text{ cm}^{-1}$ at a reference energy of 80 keV.

- [2] G. T. Herman, E. Garduño, R. Davidi, and Y. Censor. Superiorization: An optimization heuristic for medical physics. *Med. Phys.*, 39:5532–5546, 2012.
- [3] Y. Censor and T. Elfving. Block-iterative algorithms with diagonally scaled oblique projections for the linear feasibility problem. *SIAM Journal on Matrix Analysis and Applications*, 24(1):40–58, 2002.
- [4] Y. Lin and E. Samei. An efficient polyenergetic SART (pSART) reconstruction algorithm for quantitative myocardial CT perfusion. *Med. Phys.*, 41(2):021911–1 – 021911–14, 2014.
- [5] T. Humphries. Technical note: Convergence analysis of a polyenergetic SART algorithm. *Medical Physics*, 42(7):1407–1404, 2015.
- [6] P. Sukovic and N.H. Clinthorne. Penalized weighted least-squares image reconstruction for dual energy X-ray transmission tomography. *IEEE Trans. Med. Imag.*, 19(11):1075–1081, Nov 2000.
- [7] T. Humphries, J. Winn, and A. Faridani. Superiorized algorithm for reconstruction of CT images from sparse-view and limited-angle polyenergetic data. *Phys. Med. Biol.*, 62(16):6762, 2017.
- [8] J. Fessler. Michigan image reconstruction toolbox. <http://web.eecs.umich.edu/~fessler/code/>.
- [9] W.P. Segars, G. Sturgeon, S. Mendonca, J. Grimes, and B.M.W. Tsui. 4D XCAT phantom for multimodality imaging research. *Medical Physics*, 37(9):4902–4915, 2010.
- [10] W.P. Segars, M. Mahesh, T. J. Beck, E. C. Frey, and B.M.W. Tsui. Realistic CT simulation using the 4D XCAT phantom. *Medical physics*, 35(8):3800–3808, 2008.